ACS APPLIED ELECTRONIC MATERIALS

pubs.acs.org/acsaelm Article

Multiferroic h-$LuFeO_3$ Thin Films on (111) and (100) Surfaces of YSZ Substrates: An Experimental and Theoretical Study

Maria Markelova, Roy Nygaard,* Dmitry Tsymbarenko, Alyona Shurkina, Alexander Abramov, Vadim Amelichev, Artyom Makarevich, Alexander Vasiliev, and Andrey Kaul

Cite This: *ACS Appl. Electron. Mater.* 2021, 3, 1015−1022 Read Online

ACCESS | Metrics & More | Article Recommendations | Supporting Information

ABSTRACT: Thin films of in-bulk unstable multiferroic hexagonal $LuFeO_3$ were synthesized on coherent (111) and for the first time on incoherent (100) YSZ and Pt/YSZ surfaces by the metal−organic chemical vapor deposition (MOCVD) technique. The obtained films were thoroughly studied by X-ray diffraction (XRD), high-resolution transmission electron microscopy (HRTEM), scanning electron microscopy (SEM), electron backscatter diffraction (EBSD), atomic force microscopy (AFM), piezoresponse force microscopy (PFM), and theoretical simulations. The substrate surface symmetry has a crucial role in the formation of the epitaxial film's structure. Also, the molecular mechanics calculations were adapted for film/substrate interface simulation and, for the first time, the number of variants was predicted by the number of minima on the energy profile as well as it was proved that that the formation of h-$LuFeO_3$ is more energetically preferable than o-$LuFeO_3$, even on the incoherent surface. It was shown that h-$LuFeO_3$ films deposited on the YSZ(111) surface have formed a single in-plane rotational variant structure, while those deposited on the YSZ(100) surface have formed a bivariant structure. PFM results of bivariant h-$LuFeO_3$(001)//Pt(111)//YSZ(100) show half the size of ferroelectric domains (∼100 nm) and twice as large the values of piezoelectric response compared to h-$LuFeO_3$(001)//Pt(111)//YSZ(111).

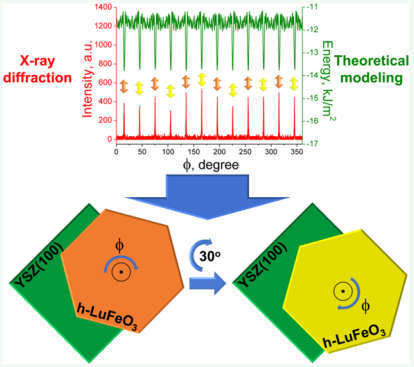

KEYWORDS: *thin films, variant structures, interface energy, MOCVD, multiferroics*

1. INTRODUCTION

In recent years, multiferroic magnetoelectric thin films have attracted great attention in the field of materials science due to their potential applications in microelectronics, spintronics, and straintronics.[1−6] In these materials the coexistence and coupling of magnetic and ferroelectric orders takes place; however, for most of the materials, such a behavior appears at low temperatures. Also, there are certain fundamental reasons why the number of magnetoelectric compounds that exhibit both orderings at room temperature is limited.[7] Recently, the hexagonal modification of $LuFeO_3$ ($P6_3cm$) has attracted great attention[8,9] since it had been shown that, being doped by Ni,[10] In,[11] and Sc,[12−14] it becomes a room-temperature magnetoelectric compound.

It should be noted that, in conditions of a common solid-state synthesis, rare-earth ferrites ($REFeO_3$) form in the thermodynamically stable structure of the orthorhombically distorted perovskite (*Pnma*), which is a simple antiferromagnetic with only a hint of the ferroelectric order.[15] Yet, the hexagonal modification may be stabilized in the shape of thin film on a surface with the certain symmetry.[16] Now, it is claimed that matching (coherent) symmetries of the coincident sites lattices (CSL) of a substrate and a film along with the optimal film/substrate crystal lattice misfit is the key to the formation of h-$REFeO_3$ phases and its epitaxial growth along the *c* axis.[17,18] Accordingly, epitaxial h-$REFeO_3$ thin films were deposited on various surfaces possessing the triangular or hexagonal symmetry such as Al_2O_3(001)[19−22] and YSZ(111).[16,23] Obviously, the strain state and the grain size in the film strongly depend upon the chosen substrate. Therefore, obtaining thin films on surfaces with incoherent or partially coherent symmetry is also of great interest since the formation of a variant structure, which strongly affects the magnetoelectric properties of the material,[24] may be expected. The growth of h-$REFeO_3$ phases on the surface with incoherent symmetry is still a challenge. Moreover, there are only few examples of thermodynamically stable hexagonal structures that were successfully deposited on the incoherent surface.[25−29]

In this study, we report the successful deposition and thorough experimental and theoretical investigation of h-$LuFeO_3$ epitaxial thin films on the surface possessing the coherent (YSZ(111)) and incoherent symmetry (YSZ(100)).

Received: December 26, 2020
Accepted: January 26, 2021
Published: February 5, 2021

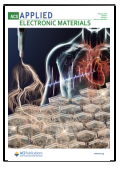

https://dx.doi.org/10.1021/acsaelm.0c01127
ACS Appl. Electron. Mater. 2021, 3, 1015−1022

Thorough investigations showed that h-$LuFeO_3$ forms a bivariant structure on the YSZ(100) surface, which is supported by the molecular mechanics calculations.

2. EXPERIMENTAL SECTION

2.1. Thin Film Growth and Investigation. All h-$LuFeO_3$ thin films were prepared by metal−organic chemical vapor deposition (MOCVD) using the experimental setup with a hot-wall vertical reactor and single flash evaporator, which is described in detail elsewhere,[16] and $Lu(thd)_3$ and $Fe(thd)_3$ (thd = 2,2,6,6-tetramethyl-heptane-3,5-dionate) as precursors. The mol ratio $Fe(thd)_3$:$Lu(thd)_3$ in the precursor mixture was optimized in the range of 0.5−2.0 in order to obtain stoichiometric single-phase films according to X-ray diffraction (XRD) and energy dispersive X-ray analysis (EDX) results in a manner similar to ref 30 and was found to be 1.1:1. The deposition temperature was 900 °C, the precursor evaporator temperature was 240 °C, the total gas pressure in the reactor was 7 mbar, and the partial oxygen pressure was 0.7 mbar. All deposition runs were carried out simultaneously on one-side polished YSZ(111) and YSZ(100) substrates fixed in parallel to the substrate holder. Commercially available epi-ready single-crystalline YSZ substrates were annealed in air for 10 h at 1100 °C prior to the deposition process to eliminate the damaged layer formed during chemical−mechanical polishing (see the atomic force microscopy (AFM) images made before and after the annealing in the Supplementary Figure S1).

Pt films were deposited on (111) and (100) YSZ surfaces by magnetron sputtering with the use of the experimental setup, which is described elsewhere.[31] The vacuum chamber was initially evacuated to a residual pressure of 10^{-6} mbar, and after that, the argon pressure of 0.07 mbar was created in order to carry out the deposition. The high purity (99.999%) platinum target with a diameter of 60 mm was used. The distance between the target and the substrate was about 5 cm, and the substrate temperature was 650 °C. The deposition rate was about 0.5 nm/s, and the final thickness of Pt films was approximately 400 nm.

The cation composition of h-$LuFeO_3$ films was checked by an EDX detector (e2v Sirius SD IXRF) in a scanning electron microscope Carl Zeiss EVO 50 SEM. The epitaxial growth of h-$LuFeO_3$ and Pt thin films was proved by XRD (out-of-plane $2\theta/\omega$, φ-scans) using the Rigaku Smartlab 5-circle X-ray diffractometer. The surface morphology and roughness of h-$LuFeO_3$ and Pt thin films and substrates were investigated with the use of scanning electron microscopy (SEM) (Helios Nanolab 660 at an accelerating voltage 2−30 kV) and AFM (NT-MDT NTegra Aura) techniques. The surface textures of h-$LuFeO_3$ films were analyzed by the electron backscatter diffraction (EBSD) method using a Jeol JSM-840A SEM and Oxford Instruments HKL Channel 5. The thickness of the h-$LuFeO_3$ thin films was determined using transmission electron microscopy (TEM) and AFM techniques. In case when AFM was used for that purpose, the film was scratched with the YSZ single crystal and then the transversal profile of the scratch was registered using an atomic force microscope.

Cross-sectional h-$LuFeO_3$(001)//YSZ specimens were prepared by the standard lift-out technique in an SEM/FIB Helios Nanolab 660 (ThermoFisher Scientific, USA), equipped with a micromanipulator Omniprobe (Omniprobe, USA) for extracting thin lamella specimens. The lamellas were studied in a Titan 80-300 TEM/STEM (FEI, USA) equipped with a spherical aberration corrector (probe corrector), with an accelerating voltage of 300 kV. The device is equipped with an EDX Si(Li) spectrometer (EDAX, USA), high-angle annular dark field (HAADF) electron detector (Fischione, USA), and Gatan Image Filter (GIF) (Gatan, USA).

Piezoresponse force microscopy (PFM) mode of the MFP-3D (Asylum Research, Oxford Instruments, UK) scanning probe microscope was used to study local piezoelectric response distribution across the surface of h-$LuFeO_3$(001)//Pt(111)//YSZ heterostructures. Measurements were done by HA_FM ETALON (NT-MDT Spectrum Instruments, Russia) probes with W2C+ coating, with a curling radius of 10−20 nm and a stiffness of 6 N/m. AC voltage (20 kHz, 5 V rms) was applied to the tip. The sample was fixed on the grounded substrate with the silver paste. The measurements were carried out at room temperature (24−28 °C), normal atmospheric pressure (1 bar), and air humidity of about 5%, which was ensured by the flow of the dry air current constantly blowing on the sample.

2.2. Theoretical Modeling of Interface Energy Profile. The interface energy was calculated with the use of the simplified universal force field (UFF) potential, which was originally developed for modeling of molecular geometry and is discussed elsewhere.[32] In order to keep the model simple, the number of factors that contribute to the total interface energy was reduced to the number of two: (1) the member that counts for covalent and ionic interaction and (2) the van der Waals interaction (see the complete set of used formulae and atomic constants in the Supporting Information). The calculation algorithm was translated into a user-written C code, which was then used for theoretical modeling.

Since the unit cells of orthorhombic and hexagonal $LuFeO_3$ modifications consist of several nonequivalent layers, all of them had to be checked in order to find the interface configuration with minimal energy. Atomic layers that were chosen for calculations are illustrated in Figure 1.

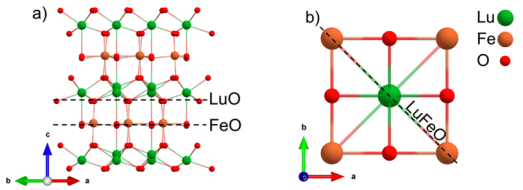

Figure 1. Depiction of the arrangement of atoms in the unit cell of the hexagonal $LuFeO_3$ (a) and in the pseudocubic unit cell of orthorhombic $LuFeO_3$ (b). Highlighted atomic layers were selected for calculation (layers are tagged according to their stoichiometry).

It should be noted here that these atomic planes were selected according to experimental data on $LuFeO_3$ film growth. Indeed, in accordance to our previous study,[16] the hexagonal modification of $LuFeO_3$ tends to grow with the [001] direction being perpendicular to the YSZ(111) substrate plane, while new experimental results have shown that h-$LuFeO_3$ grows likewise on the YSZ(100) surface. The growth of epitaxial thin films of orthorhombic modification of $LuFeO_3$ still remains poorly investigated.[15,33] However, the growth of orthorhombic rare-earth manganates is currently far better studied. It was shown that orthorhombic manganates tend to grow with their pseudocubic $[110]_p$ direction perpendicular to the YSZ(100) surface[34] and, since rare earth manganates and orthoferrites are isostructural, it seems to be reasonable to use these data as a starting point for the research.

The calculations of the interface energy, i.e., the energy gain after the film/substrate interface formation, were carried out for two disc-shaped atomic clusters (which represent the film and substrate) "cut" along crystallographic directions that were stated above. Reduced structural fragments reflecting the symmetry of the investigated systems are displayed in Figure 2 (see the full view cluster systems in Supplementary Figure S2). As a first stage of the modeling process, the film cluster was brought in contact with the substrate cluster with subsequent alignment in order to find the position with minimal interface energy. At the second stage, the film cluster was rotated around its central axis (which is called here ϕ-axis, referring to the analogy with the XRD ϕ-scanning technique) with the interface energy being calculated at each rotation step. The angle step was set at 0.1°, and the total number of steps was 3600. In order to make sure that the configuration with minimal energy obtained during the calculation is indeed a stable solution, we altered the film cluster radius, carrying out independent calculations for radii of 10, 20, 30, and 40 Å. The substrate cluster radius was kept constant (50 Å). The thickness of the substrate and film discs were also kept constant (4 Å).

https://dx.doi.org/10.1021/acsaelm.0c01127
ACS Appl. Electron. Mater. 2021, 3, 1015−1022

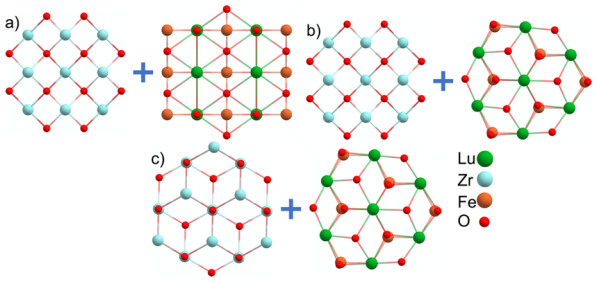

Figure 2. Visualization of reduced fragments of cluster systems under investigation: YSZ(100) + o-$LuFeO_3(110)_p$ (a); YSZ(100) + h-$LuFeO_3$(001) (b); YSZ(111) + h-$LuFeO_3$(001) (c).

3. RESULTS AND DISCUSSION

3.1. Results of Experimental Investigation of h-$LuFeO_3$ Thin Films Deposited on YSZ(111) and YSZ(100) Substrates. $2\theta/\omega$ XRD scan of $LuFeO_3$ thin films clearly indicates the sharp out-of-plane (00l) orientation of the hexagonal $LuFeO_3$ without reflexes of impurity phases on both coherent (111) and incoherent (100) YSZ surfaces (Figure 3a, black line and red line, respectively). This itself is

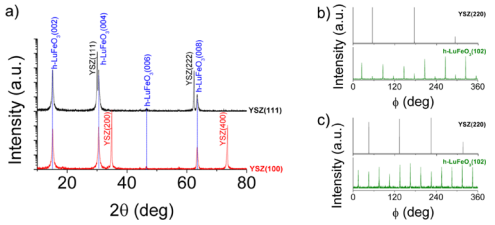

Figure 3. XRD $2\theta/\omega$ scan of the h-$LuFeO_3$ thin films on YSZ(111) (black line) and YSZ(100) (red line) substrates (a). Panels (b) and (c) correspond to ϕ-scans of {220} YSZ(111) (black line) + {102} h-$LuFeO_3$ (green line) and {220} YSZ(100) (black line) + {102} h-$LuFeO_3$ (green line), respectively.

an intriguing result since it would be more expectable if the orthorhombic modification of $LuFeO_3$ would have formed on the YSZ(100) surface as it was observed for the $LaMnO_3$/YSZ(100) interface.[34] The expectation is also associated with a relatively similar motive of the CSL and closeness of o-$LuFeO_3$ a and c parameters (5.5556 and 5.2176 Å, respectively) to a cubic parameter of YSZ (5.139 Å). The results of transmission electron microscopy and selected area diffraction additionally confirm the formation of [00l] oriented h-$LuFeO_3$ on the YSZ(100) surface (Figure 4a–d).

Additional TEM investigations allowed us to capture another several interesting structural features of the h-$LuFeO_3$(001)//YSZ(100) film. First of all, the detailed view of the intragranular border between neighbor grains (Figure 4e,f) shows that h-$LuFeO_3$ atomic planes are translated by $1/2c_{\text{h-LuFeO3}}$, which is equivalent to the 60° rotation in the $P6_3cm$ unit cell that gives rise to six reflections on the ϕ-scan of a single h-$LuFeO_3$ variant. Second, a high-resolution TEM (HRTEM) image in Figure 4g shows the presence of a particle formed on top of the YSZ(100) surface, which, according to the FFT (see the inset in Figure 4g), is the ε-Fe_2O_3 oriented with its [001] direction perpendicular to the substrate plane. This is consistent with the reported formation of the thin film ε-Fe_2O_3 stabilized on the YSZ(100) substrates.[35] Notably, h-$LuFeO_3$ formed in an oriented manner on top of the ε-Fe_2O_3 nanoparticle. There is a clear difference in the orientation of

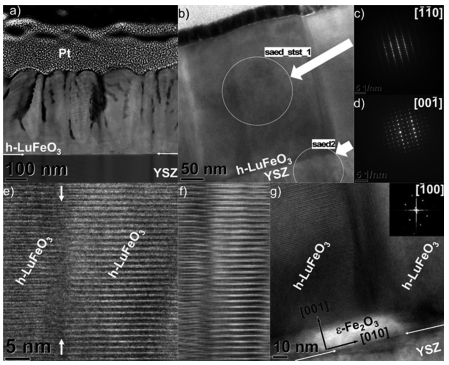

Figure 4. Results of TEM investigation of h-$LuFeO_3$(001)// YSZ(100) thin films including low-magnification HAADF STEM image (a), BFTEM image (b), selected area diffraction patterns (c, d) of the film and the substrate, HRTEM image of the antiphase border between neighbor grains of h-$LuFeO_3$ (e) and its filtered image (f), and finally the HRTEM image of the oriented ε-Fe_2O_3 particle formed on the YSZ(100) substrate (g). The inset shows the FFT from the ε-Fe_2O_3 region.

the atomic planes of the h-$LuFeO_3$ grain that formed over the ε-Fe_2O_3 and the one that began to grow from the substrate surface, which, along with the presence of the dark stressed region, indicates that these grains are rotated at a certain angle with respect to each other. To the best of our knowledge, the formation of the mixture of oriented h-$LuFeO_3$/ε-Fe_2O_3 phases has never been reported yet. The practical importance of such composites should be high since ε-Fe_2O_3 itself is a room-temperature multiferroic,[36] and thus coexistence of these two phases may greatly enhance the functional properties of the material. This point requires further investigations.

XRD data allow us to derive additional information about the similarities and differences of h-$LuFeO_3$ obtained on (111) and (100) YSZ surfaces. It is best seen on the most intensive film reflection (h-$LuFeO_3$ (002)) that the reflections of the hexagonal phase in both cases are situated on roughly the same 2θ angle (the calculated c parameter is 11.715 and 11.718 Å for h-$LuFeO_3$ deposited on YSZ(111) and YSZ(100), respectively). This observation means that drastic change of substrate symmetry in this particular case does not induce intragranular strain in the film. There is however a considerable change in FWHM: the (002) reflection of h-$LuFeO_3$(001)//YSZ(100) is 0.01° (5%) broadened compared to the (002) reflection of h-$LuFeO_3$ deposited on the YSZ(111) substrate, which may indicate the relative reduction of single-crystalline domain size of the first one. XRD ϕ-scans further reveal the intricacies of the microstructure of obtained films (Figure 3b and Figure 3c represent ϕ-scans of {220} YSZ(111)+{102} h-$LuFeO_3$(001) and {220} YSZ (100)+{102} h-$LuFeO_3$(001), respectively). First of all, these data indicate that, along with the out-of-plane orientation, there is also a sharp in-plane orientation of h-$LuFeO_3$ (the FWHM of the ϕ-scan reflection is ~0.7° for all films). Interestingly, instead of six reflections that one may expect to find on a ϕ-scan of a thin film with 6_3 axis perpendicular to the substrate surface, there are 12 reflections, which means that there are two variants, rotated by 30° with respect to each other. However, there is a difference between these ϕ-scans: while reflections of h-$LuFeO_3$(001)//YSZ(100) have roughly the same intensity, which indicates that the weight ratio of variants in this film is close to 1, in the case of h-$LuFeO_3$(001)//YSZ(111), reflection intensities of one

https://dx.doi.org/10.1021/acsaelm.0c01127
ACS Appl. Electron. Mater. 2021, 3, 1015–1022

variant noticeably dominate over the other, which hints that one variant prevails over the other.

To understand the difference, we have carried out another deposition on (111) and (100) YSZ substrates in order to obtain the films of a thickness under 100 nm, i.e., below the critical thickness of h-$LuFeO_3$. The films were studied with the EBSD technique, and the results are presented as texture maps (Figure 5a,b). We find this method excellently fitting our needs

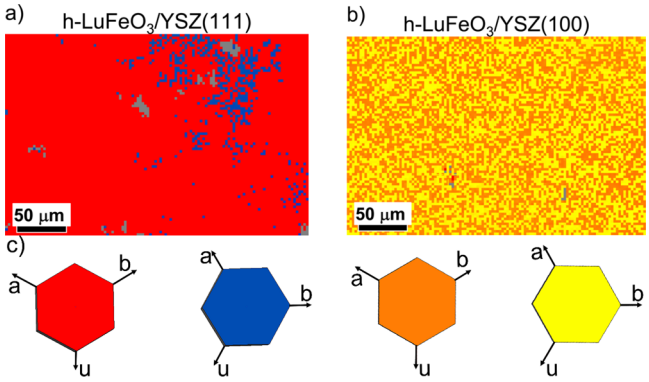

Figure 5. Results of EBSD analysis are represented as texture maps with pictures of surface disorientation of h-$LuFeO_3$ films on YSZ(111) (a) and YSZ(100) (b). Panel (c) contains the color map, revealing h-$LuFeO_3$ in-plane orientations corresponding to each color. Gray areas correspond to regions that could not be identified as any of the selected h-$LuFeO_3$ orientations.

since it is able to give information on the local orientation of the surface grains. Observed Kikuchi lines were clear and intensive, proving the high crystallinity and distinct surface orientation of h-$LuFeO_3$ films.

It should be noted that EBSD results lay in full agreement with the XRD data cornering the in-plane orientation of h-$LuFeO_3$ as well as the weight ratio of variants in films. It is clearly seen that, in the case of h-$LuFeO_3$(001)//YSZ(111), the "blue" variant is much suppressed compared to the "red" one, while in the case of h-$LuFeO_3$(001)//YSZ(100), both variants are statistically distributed across the surface. Returning back to the TEM images (Figure 4a) of the h-$LuFeO_3$(001)//YSZ(100) film, one may notice that the film has a columnar microstructure with the mean diameter of a single column being about 100 nm. Now, it is clear that these columns are in fact rotational variants of h-$LuFeO_3$.

The results of XRD and EBSD allowed us to assume the film/substrate epitaxial relations:

h-$LuFeO_3$(001)//YSZ(111)

"red" variant
$$\begin{cases} (0001)_{hex}LuFeO_3//(111)YSZ \\ \langle 1\bar{1}00\rangle_{hex}LuFeO_3//\langle 1\bar{1}0\rangle YSZ \end{cases}$$

"blue" variant
$$\begin{cases} (0001)_{hex}LuLeO_3//(111)YSZ \\ \langle \bar{1}2\bar{1}0\rangle_{hex}LuFeO_3//\langle 1\bar{1}0\rangle YSZ \end{cases}$$

h-$LuFeO_3$(001)//YSZ(100)

"orange" variant
$$\begin{cases} (0001)_{hex}LuFeO_3//(100)YSZ \\ \langle 11\bar{2}0\rangle_{hex}LuFeO_3//\langle 001\rangle YSZ \end{cases}$$

"yellow" variant
$$\begin{cases} (0001)_{hex}LuFeO_3//(100)YSZ \\ \langle \bar{1}2\bar{1}0\rangle_{hex}LuFeO_3//\langle 010\rangle YSZ \end{cases}$$

Basing on these relations, we proposed the scheme of the mutual alignment of h-$LuFeO_3$ and YSZ unit cells for both cases: h-$LuFeO_3$(001)//YSZ(111) and h-$LuFeO_3$(001)//YSZ(100) (Figure 6a and Figure 6b, respectively). Lattice mismatches were calculated using the formula

$$\left(\varepsilon = \frac{|a_{substrate} - a_{film}|}{a_{film}}\right) \quad (1)$$

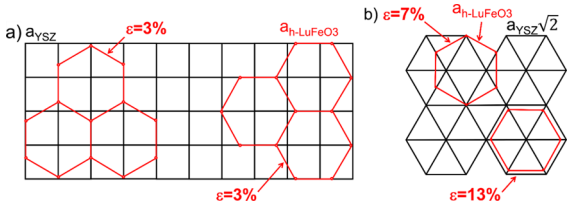

Figure 6. Scheme of the mutual alignment of h-$LuFeO_3$ and YSZ unit cells in the case of (100) (a) and (111) (b) substrate orientations. The variant with lattice mismatch ε =13% does not form.

As it is shown in Figure 6a, both variants of h-$LuFeO_3$ films on YSZ(100) have an equal lattice mismatch (~3%). These variants are energetically equivalent and thus form in a roughly equal amount, which lays in agreement with XRD ϕ-scanning and EBSD results.

Contrary to h-$LuFeO_3$(001)//YSZ(100)), one variant of h-$LuFeO_3$ on YSZ(111) has the larger modulus of lattice mismatch (~13%) than the other one (~7%) (Figure 6b). The practice of epitaxial film growth shows that 13% is an extremely large lattice mismatch,[37] which would lead to anomalously high strain in films, and thus such variant should not form at all. Our calculations that are discussed below also indicate that only one variant of h-$LuFeO_3$ is possible on the YSZ(111) surface. We assume that the second variant, which manifests as additional six reflections of low intensity on the XRD ϕ-scan and the blue colored regions on the EBSD map, forms on top of the oriented Fe_3O_4 insets reported to form on the substrate and within the film matrix during the deposition of h-$LuFeO_3$[38,39] and $LuFe_2O_4$[40] thin films. As an interim summary, it should be stressed that the difference between the microstructures of h-$LuFeO_3$ formed on two types of surfaces is that, in the case of YSZ(100) two variants, would have formed anyway, while in the case of YSZ(111), the second rotational variant forms solely due to local fluctuational formation of Fe_3O_4. These results show that the deposition of the hexagonal $LuFeO_3$ film on the surfaces of different symmetries allows us to drastically alter the microstructure of the film and thus may open the opportunity to affect structurally sensitive functional properties of the material.

Theory and practice of the epitaxial stabilization state that the thickness of the stabilized epitaxial phase is limited by the value of the critical thickness (h_c).[41−43] When the thickness of the epitaxial phase reaches h_c, the growth switches to the phase or phases, which are thermodynamically stable in the bulk state. In order to estimate and compare the critical thickness of hexagonal $LuFeO_3$ on YSZ(100) and YSZ(111) substrates, we have carried out the series of three depositions varying the thickness of films and simultaneously depositing on both

https://dx.doi.org/10.1021/acsaelm.0c01127
ACS Appl. Electron. Mater. 2021, 3, 1015−1022

substrates during each deposition run. Figure 7a and Figure 7b show XRD $2\theta/\omega$ scans of h-$LuFeO_3$ thin films deposited on

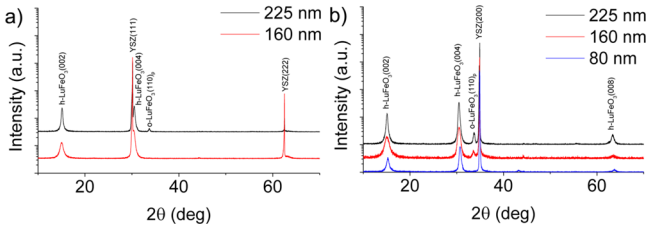

Figure 7. $2\theta/\omega$ XRD scans of h-$LuFeO_3$ of various thicknesses deposited on YSZ(111) (a) and YSZ(100) (b) substrates.

YSZ(111) and YSZ(100), respectively. It can be seen that, while the XRD pattern of the 160 nm-thick film deposited on YSZ(111) has no sign of orthorhombic modification, the film of the same thickness deposited on YSZ(100) has a well noticeable reflection of o-$LuFeO_3$, which gets more intensive with the thickness increasing. Thus, it becomes clear that, despite the fact that the YSZ(100) surface does fit for stabilizing hexagonal $LuFeO_3$, its formation on this substrate is less energetically beneficial compared to the formation on the substrate with the triangular symmetry.

Notably, the orthorhombic $LuFeO_3$ grows in an oriented manner: its pseudocubic (110) plane (which is equivalent to a (121) *Pnma* reflection) is parallel to the substrate plane and h-$LuFeO_3$(001) plane. Moreover, the scanning electron microscopy (SEM) image of the 225 nm-thick h-$LuFeO_3$ film on YSZ(100) (Figure 8a,b) clearly indicates that orthorhombic

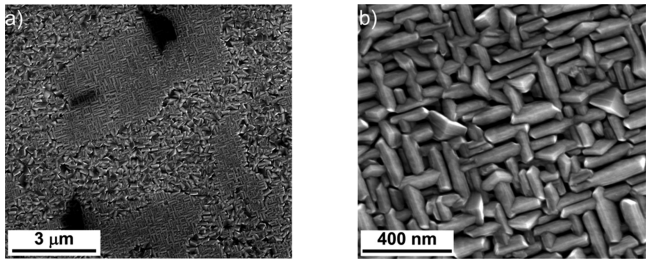

Figure 8. SEM images of 225 nm-thick h-$LuFeO_3$ film on the YSZ(100) substrate (a). Panel (b) contains the magnified region covered by the o-$LuFeO_3$ film. SEM data is consistent with the data obtained with AFM (Figure S3).

modification that is formed on top of the hexagonal one has two preferable in-plane orientations. It can also be seen that the orthorhombic phase does not cover the whole surface of the film, so it looks like after the critical thickness is exceeded the growth of the hexagonal phase does not cease completely but the mixture of these phases starts to form which has recently been shown to possess particularly interesting magnetoelectric properties.[20,44]

Finally, in order to visualize h-$LuFeO_3$ piezoelectric domains and estimate their lateral size (111) and (100) YSZ substrates, we have carried out the piezoresponse force microscopy investigations. To correctly measure the vertical polarization in the films, we had to deposit h-$LuFeO_3$ on YSZ(111) and YSZ(100) with the predeposited 400 nm-thick platinum layer. Interestingly, platinum has formed a bivariant (111)-oriented layer on the YSZ(100) substrate (see the complete XRD and AFM characterization of platinum layers in Supplementary Figures S4 and S5). The XRD $2\theta/\omega$ scans and PFM-visualized ferroelectric domains in h-$LuFeO_3$(001)//Pt(111)//YSZ-(111) and h-$LuFeO_3$(001)//Pt(111)//YSZ(100) films are shown in Figure 9a,c and Figure 9b,d, respectively.

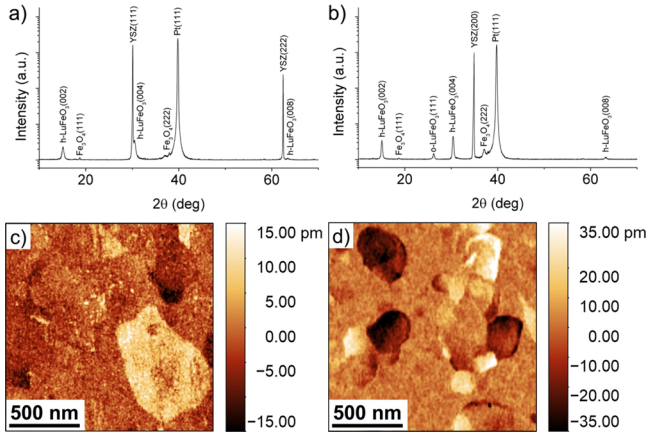

Figure 9. XRD $2\theta/\omega$ scans of h-$LuFeO_3$(001)//Pt(111)//YSZ(111) (a) and h-$LuFeO_3$(001)//Pt(111)//YSZ(100) (b) thin films. PFM images that visualize ferroelectric domains in h-$LuFeO_3$(001)//Pt(111)//YSZ(111) (c) and h-$LuFeO_3$(001)//Pt(111)//YSZ(100) (d) thin films.

The thickness of the obtained films was ∼160 nm. As it is clearly seen on $2\theta/\omega$ scans, the h-$LuFeO_3$ film has formed on both substrates. Interestingly, the reflections of an additional Fe_3O_4 phase may be observed in both cases, which is a consequence of the formation of the Pt conductive layer formed in the (111) orientation. Also, a small quantity of the orthorhombic $LuFeO_3$ phase is present in the h-$LuFeO_3$(001)//Pt(111)//YSZ(100) film, which is consistent with the results concerning the critical thickness that are discussed above.

As can be seen from Figure 9c,d, the size of ferroelectric domains in the h-$LuFeO_3$(001)//Pt(111)//YSZ(100) film is almost two times smaller than those observed in the h-$LuFeO_3$(001)//Pt(111)//YSZ(111) film. Noticeably, the lateral size of the ferroelectric domain in the h-$LuFeO_3$(001)//Pt(111)//YSZ(100) film is roughly 100 nm, which coincides with the size of a single variant observed from TEM images (Figure 4a). Also, the absolute magnitude of the piezoelectric response in the h-$LuFeO_3$(001)//Pt(111)//YSZ(100) film is more than 50% higher than the value measured in the h-$LuFeO_3$(001)//Pt(111)//YSZ(111) film. The reason of this increase needs to be clarified in further research; here, we just demonstrate the effect.

3.2. Results of Theoretical Modeling of h-LuFeO3(001)//YSZ(111), h-LuFeO3(001)//YSZ(100), and o-LuFeO3(001)//YSZ(100) Interfaces. In this study, we propose the new approach to modeling of the film/substrate systems based on the principles of molecular mechanics, harnessing the advantages of other methods (symmetry approach[45,46] and DFT calculations[47]) and lacking their weaknesses at the same time. On one hand, we are able to include both system symmetry and chemical factors (chemical bond energy) into consideration, and on the other, we are able to model systems consisting of thousands of atoms in a reasonable time. The extra benefit of using the energetic approach, which is being utilized in this research, is that, in addition to the determination of the number of rotational

https://dx.doi.org/10.1021/acsaelm.0c01127
ACS Appl. Electron. Mater. 2021, 3, 1015−1022

variants, it allows us to compare the total energy of various interfaces and thus make a definite choice as to which one is more stable in any particular case. This is shown in Figure 10a for the h-$LuFeO_3$(001)//YSZ(111) interface, Figure 10b (green) for the h-$LuFeO_3$(001)//YSZ(100) interface, and Figure 10b (red) for the o-$LuFeO_3(110)_p$//YSZ(100) interface.

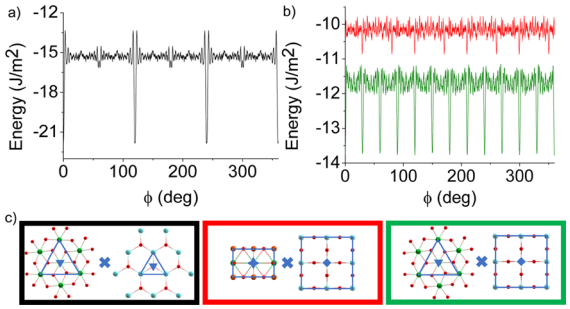

Figure 10. Calculated energy profiles obtained by rotation of the film cluster around the axis perpendicular to the substrate cluster (the ϕ-axis) for YSZ(111) (a) and YSZ(100) (b) cases. Panel (c) illustrates the interacting symmetry operations framed by colors corresponding to energy profiles. The illustration of the mutual alignment of unit cells corresponding to each energy minimum is presented in the Supporting Information (Figure S6).

In the case of interfaces with h-$LuFeO_3$, the reasonable energy profile was obtained only when the h-LuO layer (see Figure 1a) was brought into contact with the substrate, and thus only those cases are discussed here. It can be clearly seen that the energy of the h-$LuFeO_3$(001)//YSZ(100) interface demonstrates the presence of 12 sharp minima (Figure 10b, green line), which correspond to two structural variants that are rotated by 30° with respect to each other. This result coincides with experimental results of XRD ϕ-scanning (Figure 3c), and thus it becomes obvious that the formation of such a structure has thermodynamic grounding, not kinetic. We can observe the same coincidence in the case of the h-$LuFeO_3$(001)//YSZ(111) interface: there is a single structural variant that is represented by three minima on the energy profile (Figure 10a). As it was noted previously, six reflections on ϕ-scans occur due to 6_3 axis perpendicular to the substrate plane: X-ray diffraction occurs on two sets of planes that cannot be transformed one to another by a simple rotation or reflection operation. Since only one atomic plane is taken into account during the calculation, it becomes clear why we obtain three minima instead of six ones. Our calculations have also shown that the o-$LuFeO_3(110)_p$//YSZ(100) interface, if it was possible to obtain, would have consisted of two structural variants rotated by 40° with respect to each other (Figure 10b, red line), which partially coincides with the literature data concerning rare-earth manganates.[34] It also becomes obvious why h-$LuFeO_3$ forms on YSZ(100) instead of bulk-stable o-$LuFeO_3$: the minimal energy of the o-$LuFeO_3(110)_p$//YSZ(100) interface is 26.7% higher than the minimal energy of h-$LuFeO_3$(001)//YSZ(100). This finding corresponds to the fact that the thermodynamic origin of epitaxial stabilization is assumed in all the scenarios of the phenomenon.[41,42]

4. CONCLUSIONS

We have demonstrated the epitaxial stabilization of the hexagonal h-$LuFeO_3$ film on the cubic substrate with incoherent (YSZ(100)) and coherent (YSZ(111)) symmetry. Using XRD, EBSD, and TEM techniques, we have proven that h-$LuFeO_3$(001)//YSZ(100) films possess the bivariant structure: two rotational variants coexist in an otherwise epitaxial thin film. On the other hand, the h-$LuFeO_3$(001)//YSZ(111) film demonstrates the dominance of one variant over another, which is proved by the EBSD and XRD data. TEM data has revealed that, in the case of the YSZ(100) surface, the oriented ε-Fe_2O_3 inclusions form on the substrate surface and than serve for the subsequent oriented growth of h-$LuFeO_3$. This seems to be the analogy to the formation of Fe_3O_4 in h-$LuFeO_3$ films deposited on YSZ(111) substrates, which has been reported previously. Both cases are of great scientific and applicational importance since coexisting of these phases may lead to the room-temperature multiferroicity. The XRD data of the series of films with different thicknesses show that the critical thickness of h-$LuFeO_3$ on YSZ(100) is lower compared to h-$LuFeO_3$ on YSZ(111), which originates from the lower absolute value of the stabilization energy and agrees with results of molecular mechanics simulations that were performed using the algorithm adapted for the film/substrate interface simulations. It was shown that the formation of the o-$LuFeO_3(110)_p$//YSZ(100) interface gives less energy gain than the formation of h-$LuFeO_3$(001)//YSZ(100) interface. The practical application of magnetoelectric materials requires a conductive sublayer, which, in the case of metastable h-$LuFeO_3$, should have a crucial role in epitaxial stabilization. We have selected the oriented platinum layer as a conductive epitaxial electrode and successfully achieved the epitaxial stabilization of h-$LuFeO_3$ on Pt(111)/YSZ with both substrate orientations. The results of PMF measurements of these heterostructures have shown that the lateral size of ferroelectric domains in h-$LuFeO_3$(001)//Pt(111)//YSZ(100) is half the size of domains in h-$LuFeO_3$(001)//Pt(111)//YSZ(111), which is obvious since the size of the ferroelectric domain typically coincides to the size of the grain. At the same time, the piezoelectric response in h-$LuFeO_3$(001)//Pt(111)//YSZ(100) shows to be almost twice as large as the piezoelectric response in h-$LuFeO_3$(001)//Pt(111)//YSZ-(111), which may find further application in the industry.

■ ASSOCIATED CONTENT

Supporting Information

The Supporting Information is available free of charge at https://pubs.acs.org/doi/10.1021/acsaelm.0c01127.

Formulas and atomic constants that were used in theoretical modeling of interfaces (Table S1); AFM images of YSZ single-crystalline substrates before (Figure S1a and Figure S1c, respectively) and after the annealing (Figure S1b and Figure S1d, respectively); the view from above and the side view of the h-$LuFeO_3$(001)+YSZ(111) cluster system (Figure S2a and Figure S2b, respectively), h-$LuFeO_3$(001)+YSZ(100) cluster system (Figure S2c and Figure S2d, respectively), and o-$LuFeO_3(110)_p$+YSZ(100) cluster system (Figure S2e and Figure S2f, respectively); AFM images of h-$LuFeO_3$(001)//YSZ(111) and h-$LuFeO_3$(001)//YSZ(100) thin films (Figure S3a and Figure S3b, respectively); XRD $2\theta/\omega$ scans (Figure S4a) and ϕ-scans (Figure S4b and Figure S4c) of Pt(111)//YSZ(111) and Pt(111)//YSZ(100) films; AFM images of these films (Figure S5a and Figure S5b, respectively);

https://dx.doi.org/10.1021/acsaelm.0c01127
ACS Appl. Electron. Mater. 2021, 3, 1015−1022

and visualizations of the mutual alignment of unit cells derived from calculations of h-$LuFeO_3$(001)+YSZ(100), h-$LuFeO_3$(001)+YSZ(111), and o-$LuFeO_3(110)_p$+YSZ-(100) interfaces (Figure S6a, Figure S6b, and Figure S6c, respectively) (PDF)

AUTHOR INFORMATION

Corresponding Author

Roy Nygaard − *Department of Chemistry, Lomonosov Moscow State University, Moscow 119991, Russia;* orcid.org/0000-0002-0989-0826; Email: rnygaard@mail.ru

Authors

Maria Markelova − *Department of Chemistry, Lomonosov Moscow State University, Moscow 119991, Russia*

Dmitry Tsymbarenko − *Department of Chemistry, Lomonosov Moscow State University, Moscow 119991, Russia*

Alyona Shurkina − *Department of Chemistry, Lomonosov Moscow State University, Moscow 119991, Russia*

Alexander Abramov − *School of Natural Sciences and Mathematics, Ural Federal University, Ekaterinburg 620000, Russia*

Vadim Amelichev − *S-Innovations LLC, Moscow 117246, Russia*

Artyom Makarevich − *Department of Chemistry, Lomonosov Moscow State University, Moscow 119991, Russia*

Alexander Vasiliev − *National Research Centre "Kurchatov Institute", Moscow 123182, Russia; Shubnikov Crystallography Institute of the Russian Academy of Sciences, Moscow 119333, Russia*

Andrey Kaul − *Department of Chemistry, Lomonosov Moscow State University, Moscow 119991, Russia*

Complete contact information is available at: https://pubs.acs.org/10.1021/acsaelm.0c01127

Author Contributions

A.K. conceived the idea and supervised the project. M.M., A.S., and R.N. carried out MOCVD depositions. V.A., A.M., D.T. collected the data for films characterization by XRD, EBSD and AFM methods, R.N. and M.M. interpreted the data. A.A. carried out PFM studies of thin films. A.V. performed TEM studies. D.T. and R.N. developed the code, performed molecular mechanics calculations and interpreted experimental and theoretical data. R.N. took the lead in writing of the manuscript with contributions from D.T., M.M., and A.K. All authors have given approval to the final version of the manuscript. All authors have given approval to the final version of the manuscript. Authors are grateful to SE (ResearcherID: E-1689-2012) for conducting the magnetron sputtering of Pt thin films.

Funding

Authors acknowledge the Russian Foundation for Basic Research for financial support: the MOCVD deposition experiments were conducted thanks to the financial support of the RFBR project no. 19-33-90289, and theoretical investigations and mathematical calculations became possible thanks to the RFBR project no. 20-33-70096.

Notes

The authors declare no competing financial interest.

The initial code of the calculation algorithm is available upon request from the author.

REFERENCES

(1) Schmid, H. Multi-Ferroic Magnetoelectrics. *Ferroelectrics* **1994**, *162*, 317−338.

(2) Eerenstein, W.; Mathur, N. D.; Scott, J. F. Multiferroic and Magnetoelectric Materials. *Nature* **2006**, *442*, 759−765.

(3) Van Aken, B. B.; Palstra, T. T. M.; Filippetti, A.; Spaldin, N. A. The Origin of Ferroelectricity in Magnetoelectric $YMnO_3$. *Nat. Mater.* **2004**, *3*, 164−170.

(4) Spaldin, N. A.; Ramesh, R. Advances in Magnetoelectric Multiferroics. *Nat. Mater.* **2019**, *18*, 203−212.

(5) Béa, H.; Gajek, M.; Bibes, M.; Barthélémy, A. Spintronics with Multiferroics. *J. Phys. Condens. Matter* **2008**, *20*, 434221.

(6) Roy, K. Ultra-Low-Energy Straintronics Using Multiferroic Composites. *Spin* **2013**, *03*, 1330003.

(7) Hill, N. A. Why Are There so Few Magnetic Ferroelectrics? *J. Phys. Chem. B* **2000**, *104*, 6694−6709.

(8) Zhao, H. J.; Ren, W.; Yang, Y.; Íñiguez, J.; Chen, X. M.; Bellaiche, L. Near Room-Temperature Multiferroic Materials with Tunable Ferromagnetic and Electrical Properties. *Nat. Commun.* **2014**, *5*, 4021.

(9) Vopson, M. M. Fundamentals of Multiferroic Materials and Their Possible Applications. *Crit. Rev. Solid State Mater. Sci.* **2015**, *40*, 223−250.

(10) Suresh, P.; Vijaya Laxmi, K.; Anil Kumar, P. S. Enhanced Room Temperature Multiferroic Characteristics in Hexagonal $LuFe_{1-x}Ni_xO_3$ (x = 0 − 0.3) Nanoparticles. *J. Magn. Magn. Mater.* **2018**, *448*, 117−122.

(11) Liu, J.; Sun, T. L.; Liu, X. Q.; Tian, H.; Gao, T. T.; Chen, X. M. A Novel Room-Temperature Multiferroic System of Hexagonal $Lu_{1-x}In_xFeO_3$. *Adv. Funct. Mater.* **2018**, *28*, 1706062.

(12) Leiner, J. C.; Kim, T.; Park, K.; Oh, J.; Perring, T. G.; Walker, H. C.; Xu, X.; Wang, Y.; Cheong, S.-W.; Park, J.-G. Magnetic Excitations in the Bulk Multiferroic Two-Dimensional Triangular Lattice Antiferromagnet (Lu,Sc)FeO_3. *Phys. Rev. B* **2018**, *98*, 134412.

(13) Du, K.; Gao, B.; Wang, Y.; Xu, X.; Kim, J.; Hu, R.; Huang, F.-T.; Cheong, S.-W. Vortex Ferroelectric Domains, Large-Loop Weak Ferromagnetic Domains, and Their Decoupling in Hexagonal (Lu,Sc)FeO_3. *npj Quantum Mater.* **2018**, *3*, 33.

(14) Lin, L.; Zhang, H. M.; Liu, M. F.; Shen, S.; Zhou, S.; Li, D.; Wang, X.; Yan, Z. B.; Zhang, Z. D.; Zhao, J.; Dong, S.; Liu, J.-M. Hexagonal Phase Stabilization and Magnetic Orders of Multiferroic $Lu_{1-x}Sc_xFeO_3$. *Phys. Rev. B* **2016**, *93*, No. 075146.

(15) Mamedov, D. V.; Gavrilova, T. P.; Yatsyk, I. V.; Gilmutdinov, I. F.; Seidov, Z. Y.; Aljanov, M. A.; Najafzade, M. J.; Ibrahimov, I. N.; Chichkov, V. I.; Andreev, N. V.; Koroleva, E. Y.; Eremina, R. M. Magnetic and Dielectric Properties of O-LuFeO3/$SrTiO_3$. In *Journal of Physics Conference Series*; IOP Publishing: 2017; *903* (1), DOI: 10.1088/1742-6596/903/1/012014.

(16) Bossak, A. A.; Graboy, I. E.; Gorbenko, O. Y.; Kaul, A. R.; Kartavtseva, M. S.; Svetchnikov, V. L.; Zandbergen, H. W. XRD and HREM Studies of Epitaxially Stabilized Hexagonal Orthoferrites $RFeO_3$ (R = Eu-Lu). *Chem. Mater.* **2004**, *16*, 1751−1755.

(17) Iida, H.; Koizumi, T.; Uesu, Y.; Kohn, K.; Ikeda, N.; Mori, S.; Haumont, R.; Janolin, P.-E.; Kiat, J.-M.; Fukunaga, M.; Noda, Y. Ferroelectricity and Ferrimagnetism of Hexagonal $YbFeO_3$ Thin Films. *J. Phys. Soc. Jpn.* **2012**, *81*, 024719.

(18) Akbashev, A. R.; Roddatis, V. V.; Vasiliev, A. L.; Lopatin, S.; Semisalova, A. S.; Perov, N. S.; Amelichev, V. A.; Kaul, A. R. Reconstructed Stacking Faults in Cobalt-Doped Hexagonal $LuFeO_3$ Revealed by Mapping of Cation Distribution at the Atomic Scale. *CrystEngComm* **2012**, *14*, 5373−5376.

(19) Wang, W.; Zhao, J.; Wang, W.; Gai, Z.; Balke, N.; Chi, M.; Lee, H. N.; Tian, W.; Zhu, L.; Cheng, X.; Keavney, D. J.; Yi, J.; Ward, T. Z.; Snijders, P. C.; Christen, H. M.; Wu, W.; Shen, J.; Xu, X. Room-Temperature Multiferroic Hexagonal LuFeO3 Films. *Phys. Rev. Lett.* **2013**, *110*, 237601.

(20) Cao, S.; Zhang, X.; Sinha, K.; Wang, W.; Wang, J.; Dowben, P. A.; Xu, X. Phase Separation in $LuFeO_3$ Films. *Appl. Phys. Lett.* **2016**, *108*, 202903.

(21) Wang, W.; Wang, H.; Xu, X.; Zhu, L.; He, L.; Wills, E.; Cheng, X.; Keavney, D. J.; Shen, J.; Wu, X.; Xu, X. Crystal Field Splitting and Optical Bandgap of Hexagonal $LuFeO_3$ Films. *Appl. Phys. Lett.* **2012**, *101*, 241907.
(22) Jeong, Y. K.; Lee, J.-H.; Ahn, S.-J.; Song, S.-W.; Jang, H. M.; Choi, H.; Scott, J. F. Structurally Tailored Hexagonal Ferroelectricity and Multiferroism in Epitaxial $YbFeO_3$ Thin-Film Heterostructures. *J. Am. Chem. Soc.* **2012**, *134*, 1450−1453.
(23) Akbashev, A. R.; Semisalova, A. S.; Perov, N. S.; Kaul, A. R. Weak Ferromagnetism in Hexagonal Orthoferrites $RFeO_3$ (R = Lu, Er-Tb). *Appl. Phys. Lett.* **2011**, *99*, 122502.
(24) Lu, J.; Günther, A.; Schrettle, F.; Mayr, F.; Krohns, S.; Lunkenheimer, P.; Pimenov, A.; Travkin, V. D.; Mukhin, A. A.; Loidl, A. On the Room Temperature Multiferroic $BiFeO_3$: Magnetic, Dielectric and Thermal Properties. *Eur. Phys. J. B* **2010**, *75*, 451−460.
(25) Kang, B. S.; Stan, L.; Usov, I. O.; Lee, J.-K.; Harriman, T. A.; Lucca, D. A.; Depaula, R. F.; Arendt, P. N.; Nastasi, M.; MacManus-Driscoll, J. L.; Park, B. H.; Jia, Q. Strain Mismatch Induced Tilted Heteroepitaxial (000l) Hexagonal ZnO Films on (001) Cubic Substrates. *Adv. Eng. Mater.* **2011**, *13*, 1142−1145.
(26) Zhou, H.; Wang, H.-Q.; Li, Y.; Li, K.; Kang, J.; Zheng, J.-C.; Jiang, Z.; Huang, Y.; Wu, L.; Zhang, L.; Kisslinger, K.; Zhu, Y. Evolution of Wurtzite ZnO Films on Cubic MgO (001) Substrates: A Structural, Optical, and Electronic Investigation of the Misfit Structures. *ACS Appl. Mater. Interfaces* **2014**, *6*, 13823−13832.
(27) Sieber, H.; Senz, S.; Hesse, D. Crystallographic Orientation and Morphology of Epitaxial In2O3 Thin Films Grown on MgO(001) Single Crystal Substrates. *Thin Solid Films* **1997**, *303*, 218−221.
(28) Lee, M. K.; Eom, C. B.; Lettieri, J.; Scrymgeour, I. W.; Schlom, D. G.; Tian, W.; Pan, X. Q.; Ryan, P. A.; Tsui, F. Epitaxial Thin Films of Hexagonal $BaRuO_3$ on (001) SrTiO3. *Appl. Phys. Lett.* **2001**, *78*, 329−331.
(29) Wei, Y.; Nukala, P.; Salverda, M.; Matzen, S.; Zhao, H. J.; Momand, J.; Everhardt, A. S.; Agnus, G.; Blake, G. R.; Lecoeur, P.; Kooi, B. J.; Íñiguez, J.; Dkhil, B.; Noheda, B. A Rhombohedral Ferroelectric Phase in Epitaxially Strained $Hf_{0.5}Zr_{0.5}O_2$ Thin Films. *Nat. Mater.* **2018**, *17*, 1095−1100.
(30) Nikolaeva, A.; Nygaard, R.; Martynova, I.; Tsymbarenko, D. Synthesis, Structure and Thermal Behavior of Volatile Mononuclear Mixed Ligand Complexes of Rare-Earth Dipivaloylmethanates with Diethylenetriamine. *Polyhedron* **2020**, *180*, 114373.
(31) Khmelnitsky, R. A.; Evlashin, S. A.; Martovitsky, V. P.; Pastchenko, P. V.; Dagesian, S. A.; Alekseev, A. A.; Suetin, N. V.; Gippius, A. A. Heteroepitaxy of Ni-Based Alloys on Diamond. *Cryst. Growth Des.* **2016**, *16*, 1420−1427.
(32) Rappe, A. K.; Casewit, C. J.; Colwell, K. S.; Goddard, W. A., III; Skiff, W. M. UFF, a full periodic table force field for molecular mechanics and molecular dynamics simulations. *J. Am. Chem. Soc.* **1992**, *114*, 10024−10035.
(33) Zhu, L.; Deng, H.; Liu, J.; Sun, L.; Yang, P.; Jiang, A.; Chu, J. Preparation and Characterization of Bi-Doped $LuFeO_3$ Thin Fi Lms Grown on $LaNiO_3$ Substrate. *J. Cryst. Growth* **2014**, *387*, 6−9.
(34) Gorbenko, O. Y.; Kaul, A. R.; Bosak, A. A.; Graboy, I. E.; Zandbergen, H. W.; Svetchnikov, V. L.; Babushkina, N. A.; Belova, L. M.; Kugel, K. I. $(La1\text{-}_xPr_x)0.7Ca_{0.3}MnO_3$ Colossal Magnetoresistive Thin Films on Yttria Stabilized Zirconia. *Solid State Commun.* **2000**, *114*, 407−412.
(35) Corbellini, L.; Lacroix, C.; Harnagea, C.; Korinek, A.; Botton, G. A.; Ménard, D.; Pignolet, A. Epitaxially Stabilized Thin Films of ϵ-Fe_2O_3 (001) Grown on YSZ (100). *Sci. Rep.* **2017**, *7*, 3712.
(36) Katayama, T.; Yasui, S.; Hamasaki, Y.; Osakabe, T.; Itoh, M. Chemical Tuning of Room Terature Ferrimagnetism and Ferroelectricity in ϵ-Fe_2O_3-Type Multiferroic Oxide Thin Films. *J. Mater. Chem. C* **2017**, *5*, 12597−12601.
(37) Rasic, D.; Narayan, J. Epitaxial Growth of Thin Films. In *Crystal Growth*; Glebovsky, J. N. E.-V., Ed.; IntechOpen: Rijeka, 2019; pp. 127−212, DOI: 10.5772/intechopen.82745.
(38) Moyer, J. A.; Misra, R.; Mundy, J. A.; Brooks, C. M.; Heron, J. T.; Muller, D. A.; Schlom, D. G.; Schiffer, P. Intrinsic Magnetic Properties of Hexagonal LuFeO3 and the Effects of Nonstoichiometry. *APL Mater.* **2014**, *2*, No. 012106.
(39) Akbashev, A. R.; Roddatis, V. V.; Vasiliev, A. L.; Lopatin, S.; Amelichev, V. A.; Kaul, A. R. Reconstruction of the Polar Interface between Hexagonal $LuFeO_3$ and Intergrown Fe_3O_4 Nanolayers. *Sci. Rep.* **2012**, *2*, 672.
(40) Liu, J.; Wang, Y.; Dai, J. Y. Structural and Dielectric Properties of LuFe2O4 Thin Films Grown by Pulsed-Laser Deposition. *Thin Solid Films* **2010**, *518*, 6909−6914.
(41) Gorbenko, O. Y.; Samoilenkov, S. V.; Graboy, I. E.; Kaul, A. R. Epitaxial Stabilization of Oxides in Thin Films. *Chem. Mater.* **2002**, *33*, 4026−4043.
(42) Kaul, A. R.; Gorbenko, O. Y.; Kamenev, A. A. The Role of Heteroepitaxy in the Development of New Thin-Film Oxide-Based Functional Materials. *Russ. Chem. Rev.* **2004**, *73*, 861−880.
(43) Little, S.; Zangwill, A. Equilibrium Microstructure of Epitaxial Thin Films. *Phys. Rev. B* **1994**, *49*, 16659−16669.
(44) Song, S.; Han, H.; Jang, H. M.; Kim, Y. T.; Lee, N. S.; Park, C. G.; Kim, J. R.; Noh, T. W.; Scott, J. F. Implementing Room-Temperature Multiferroism by Exploiting Hexagonal-Orthorhombic Morphotropic Phase Coexistence in LuFeO3 Thin Films. *Adv. Mater.* **2016**, *28*, 7430−7435.
(45) Grundmann, M.; Böntgen, T.; Lorenz, M. Occurrence of Rotation Domains in Heteroepitaxy. *Phys. Rev. Lett.* **2010**, *105*, 146102.
(46) Grundmann, M. Formation of Epitaxial Domains: Unified Theory and Survey of Experimental Results. *phys. status solidi (b)* **2011**, *248*, 805−824.
(47) Xu, Z.; Salvador, P.; Kitchin, J. R. First-Principles Investigation of the Epitaxial Stabilization of Oxide Polymorphs: TiO_2 on $(Sr,Ba)TiO_3$. *ACS Appl. Mater. Interfaces* **2017**, *9*, 4106−4118.

https://dx.doi.org/10.1021/acsaelm.0c01127
ACS Appl. Electron. Mater. 2021, 3, 1015−1022